Eur. Phys. J. A (2025) 61:92
https://doi.org/10.1140/epja/s10050-025-01557-x

THE EUROPEAN PHYSICAL JOURNAL A

Regular Article - Theoretical Physics

Nucleon gravitational form factors

Z.-Q. Yao[1,2,a], **Y.-Z. Xu**[1,2], **D. Binosi**[3], **Z.-F. Cui**[4,5], **M. Ding**[4,5,b], **K. Raya**[1], **C. D. Roberts**[4,5,c], **J. Rodríguez-Quintero**[1], **S. M. Schmidt**[6,7]

[1] Dpto. Ciencias Integradas, Centro de Estudios Avanzados en Fis., Mat. y Comp., Fac. Ciencias Experimentales, Universidad de Huelva, 21071 Huelva, Spain
[2] Dpto. Sistemas Físicos, Químicos y Naturales, Univ., Pablo de Olavide, 41013 Sevilla, Spain
[3] European Centre for Theoretical Studies in Nuclear Physics and Related Areas (ECT*), Villa Tambosi, Strada delle Tabarelle 286, 38123 Villazzano, TN, Italy
[4] School of Physics, Nanjing University, Nanjing, Jiangsu 210093, China
[5] Institute for Nonperturbative Physics, Nanjing University, Nanjing 210093, Jiangsu, China
[6] Helmholtz-Zentrum Dresden-Rossendorf, Bautzner Landstraße 400, 01328 Dresden, Germany
[7] Technische Universität Dresden, 01062 Dresden, Germany

Received: 2 April 2025 / Accepted: 4 April 2025

Abstract A symmetry-preserving analysis of strong interaction quantum field equations is used to complete a unified treatment of pion, kaon, and nucleon electromagnetic and gravitational form factors. Findings include a demonstration that the pion near-core pressure is roughly twice that in the proton, so both are significantly greater than that of a neutron star; parton species separations of the nucleon's three gravitational form factors, in which, *inter alia*, the glue-to-quark ratio for each form factor is seen to take the same constant value, independent of momentum transfer; and a determination of proton radii orderings, with the mechanical (normal force) radius being less than the mass-energy radius, which is less than the proton charge radius. This body of predictions should prove useful in an era of experiments that will enable them to be tested.

1 Introduction

The nucleon mass, m_N, is a defining scale in Nature. In fact, one understands the origin of almost all mass that is visible in the Universe if one grasps the source of m_N. In modern high-energy physics, approximately 98% of m_N is expected to be generated by Standard Model strong interactions, *i.e.*, to emerge from quantum chromodynamics (QCD) [1–5]. The small remainder owes to Higgs boson couplings into QCD.

These statements are a succinct expression of an emergent hadron mass (EHM) paradigm, developed via insightful use of continuum Schwinger function methods (CSMs) – see Ref. [6] and citations thereof. The three pillars of EHM are appearance of a gluon mass scale [7], infrared saturation and cessation of running in QCD's effective charge [8], and dynamical chiral symmetry breaking expressed in a nonzero chiral-limit running quark mass [9,10]. This paradigm is drawing support from results obtained using realistic simulations of lattice-regularised QCD (lQCD) [1–5] and being/will be tested by comparisons between EHM-based predictions and data from ongoing/anticipated experiments [11–16].

Regarding pion, kaon, and nucleon electromagnetic form factors, comparisons with data are already possible. They support the EHM picture [17,18]. Additional confirmation is provided by comparisons between CSM predictions of pion gravitational form factors [19] and recent lQCD results [20] – see Ref. [5, Fig. 12]. Validated predictions for nucleon gravitational form factors would add much to the accumulating store of successes, especially if both the complete form factors and their parton decompositions were confirmed. In these contexts, some empirical information may already be available [21–23]. Moreover, lQCD has delivered results at a simulation pion mass of ≈ 0.17 GeV [24].

Section 2 introduces the Poincaré-covariant form of the in-nucleon expectation value of the QCD energy-momentum tensor and, therewith, the three observable nucleon gravitational form factors: mass, spin, and pressure. A continuum approach to the calculation of these form factors is detailed in Sect. 3. It introduces the Schwinger functions needed and

[a] e-mail: zhaoqian.yao@dci.uhu.es
[b] e-mail: mhding@nju.edu.cn
[c] e-mail: cdroberts@nju.edu.cn (corresponding author)

Published online: 02 May 2025

the manner by which reliable results can be obtained for each of them. Section 4 discusses the predictions that are subsequently obtained for each of the nucleon gravitational form factors, placing them in context with available empirical inferences and extant results from lQCD. An array of density profiles (energy, pressure, shear and normal force distributions) are described in Sect. 5. Section 6 presents a summary and perspective.

2 Nucleon gravitational current

The proton (nucleon) has three gravitational form factors, which express all objective dynamical information that can be gleaned from its interaction with a $J^{PC} = 2^{++}$ probe. They are defined via the current that describes the associated scattering process, which may be written thus:

$$\begin{aligned} m_N \Lambda^{Ng}_{\mu\nu}(Q) = &-\Lambda_+(p_f)[K_\mu K_\nu A(Q^2) \\ &+ i K_{\{\mu}\sigma_{\nu\}\rho} Q_\rho J(Q^2) \\ &+ \tfrac{1}{4}(Q_\mu Q_\nu - \delta_{\mu\nu} Q^2) D(Q^2)]\Lambda_+(p_i)\,, \end{aligned} \quad (1)$$

where $p_{i,f}$ are the momenta of the incoming/outgoing nucleon, $p^2_{i,f} = -m_N^2$, $K = (p_i + p_f)/2$, $Q = p_f - p_i$; all Dirac matrices are standard [6, Sec. 2.3], with $\sigma_{\mu\nu} = (i/2)[\gamma_\mu, \gamma_\nu]$; Λ_+ is the projection operator that delivers a positive energy nucleon; and $a_{\{\mu} b_{\nu\}} = (a_\mu b_\nu + a_\nu b_\mu)/2$.

In Eq. (1) [25]: A is the nucleon mass distribution form factor; J relates to the nucleon spin distribution; and D provides information on in-nucleon pressure and shear forces. A fourth form factor, often written $\bar{c}(Q^2)$, is identically zero owing to current conservation. In the forward limit, $Q^2 = 0$, symmetries entail $A(0) = 1$, $J(0) = 1/2$. $D(0)$ is also a conserved charge, but like the axial charge, g_A, its value is a dynamical property of the nucleon. It has been described as the "last unknown global property" of the nucleon [25]; hence, a robust prediction of $D(0)$ is critical.

3 Continuum calculation of form factors

3.1 Nucleon Faddeev wave function

Hereafter we describe a calculation of nucleon gravitational form factors using the same approach employed for pion, kaon, and nucleon electromagnetic form factors [17,18] and pion and kaon gravitational form factors [19]. Namely, we work at leading-order in a symmetry-preserving, systematically-improvable truncation of all quantum field equations which appear in the seven-point Schwinger function that corresponds to the current in Eq. (1). This is the rainbow-ladder (RL) truncation.

After almost thirty years of use [26,27], RL truncation is known to be quantitatively reliable for pion, kaon, and nucleon observables: (*a*) practically, owing to widespread, successful applications [1,3,5]; and (*b*) because improvement schemes are available and have been tested, showing that the cumulative effect of improvement to RL truncation in these channels can be absorbed into a modest modification of the quark + quark scattering kernel [28–35]. Importantly, where reasonable comparisons are possible, contemporary CSM predictions and lQCD results are mutually consistent – see, *e.g.*, Refs. [1–5,36–41].

It is worth explaining here why and where RL truncation is successful. Consider, therefore, that in systems for which nonperturbative EHM-generated feedback is small, *viz.* ground-state channels [29,35], corrections to RL truncation may be considered diagram by diagram and cancellations can algebraically be demonstrated between new terms at each given order. The remainder are small because: (*a*) QCD's effective charge is bounded above by π at infrared momenta and falls monotonically from its maximum with increasing values of its spacelike argument [8,42,43]; and (*b*) this ensures phase-space suppression is an effective mechanism for damping correction contributions.

In RL truncation, the nucleon wave function is obtained by solving the Faddeev equation depicted in Fig. 1 [44–47]. It is constructed using the Bethe-Salpeter kernel, $\mathcal{K}$, discussed below, and the dressed light-quark propagator, which has the general form

$$S(k) = 1/[i\gamma \cdot k A(k^2) + \mathbf{1} B(k^2)] \quad (2)$$

and is obtained by solving the quark gap equation defined by $\mathcal{K}$. Discussions of the formulation and solution of the linear, homogeneous Faddeev integral equation are provided, *e.g.*, in Refs. [44–47]. The output is the nucleon Faddeev amplitude, which can be used to compute all form factor matrix elements, electromagnetic, weak, gravitational, etc. In any such calculation, the amplitude must be normalised. The canonically normalised amplitude ensures, *e.g.*, that the proton electric charge is unity.

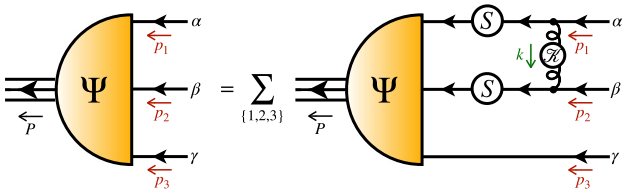

Fig. 1 Faddeev equation. Filled semicircle: Faddeev amplitude, Ψ, the matrix-valued solution, which involves 128 independent scalar functions. Spring: dressed-gluon interaction that mediates quark + quark scattering, Eq. (2). Solid line: dressed-quark propagator, S, calculated from the rainbow gap equation. Lines not adorned with a shaded circle are amputated. Isospin symmetry is assumed

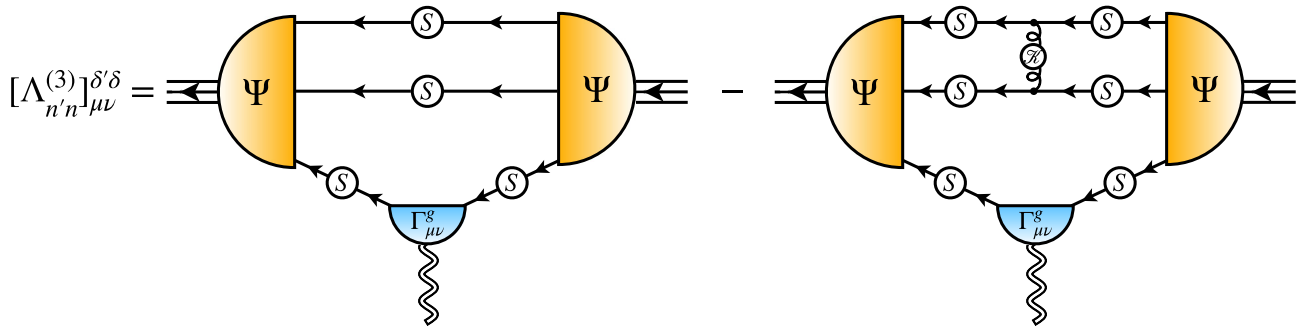

Fig. 2 $a = 3$ spinor component of the nucleon current associated with the energy-momentum tensor, where δ, δ' are spinor indices and n, n' are isospin indices. $\mathcal{K}$ indicates the Bethe-Salpeter kernel, also used to define the RL truncation gap equation that yields the dressed light-quark propagator, S, as its solution. Together, these elements complete the kernel in the Faddeev equation that yields Ψ, the nucleon Faddeev amplitude – see Fig. 1. The remaining element is $\Gamma^g_{\mu\nu}$, the dressed-graviton + quark vertex, obtained following Ref. [19]. The complete current has three terms: $\Lambda_{\mu\nu}(Q) = \sum_{a=1,2,3} \Lambda^a_{\mu\nu}(Q)$; but using symmetries, one can readily obtain the $a = 1, 2$ components of the current once $a = 3$ is known – see Ref. [48, Appendix B]

The key element in Fig. 1 is the quark + quark scattering kernel [49]:

$$\mathcal{K}^{rs}_{tu}(k) = \tilde{\mathcal{G}}(y) T_{\mu\nu}(k) \left[i\gamma_\mu \frac{\lambda^a}{2} \right]_{ts} \left[i\gamma_\nu \frac{\lambda^a}{2} \right]_{ur} , \tag{3}$$

$k^2 T_{\mu\nu}(k) = k^2 \delta_{\mu\nu} - k_\mu k_\nu$, $y = k^2$. The tensor structure specifies Landau gauge, used because, *inter alia*, it is a fixed point of the renormalisation group and that gauge for which corrections to RL truncation are minimised [50]. In Eq. (3), r, s, t, u represent colour and spinor matrix indices.

Working from studies of QCD's gauge sector, one arrives at the following practicable completion of the scattering kernel [31,51]:

$$\tilde{\mathcal{G}}(y) = \frac{8\pi^2}{\omega^4} D e^{-y/\omega^2} + \frac{8\pi^2 \gamma_m \mathcal{F}(y)}{\ln\left[\tau + (1 + y/\Lambda^2_{\rm QCD})^2\right]} , \tag{4}$$

where $\gamma_m = 12/25$, $\Lambda_{\rm QCD} = 0.234\,$GeV, $\tau = {\rm e}^2 - 1$, and $\mathcal{F}(y) = \{1 - \exp(-y/\Lambda_I^2)\}/y$, $\Lambda_I = 1\,$GeV. Analyses of gauge-sector dynamics and numerous hadron properties indicate $\omega = 0.8\,$GeV, $\omega D = 0.8\,$GeV^3 [19,35]. When the product ωD is kept fixed, physical observables relevant herein remain practically unchanged under $\omega \to (1 \pm 0.2)\omega$ [52]; thus, ω is the only degree of freedom. (Insights into the gauge-sector context of Eq. (4) are drawn in Appendix A.)

Numerical methods for solving sets of coupled gap and Faddeev equations are described elsewhere – see, *e.g.*, Refs. [45,49,53,54]. Exploiting these schemes, one may solve all equations relevant to calculation of the current in Eq. (1) and thereby arrive at predictions for the nucleon gravitational form factors.

As in Refs. [17,18], using Eq. (4) with renormalisation point invariant quark current mass $\hat{m}_u = \hat{m}_d = 6.04\,$MeV, which corresponds to a one-loop mass at $\zeta = \zeta_2 := 2\,$GeV of 4.19 MeV, one finds: pion mass $m_\pi = 0.14\,$GeV; nucleon mass $m_N = 0.94\,$GeV; and pion leptonic decay constant $f_\pi = 0.094\,$GeV. These values align with experiment [55].

The scattering kernel involves one parameter and there is a single quark current-mass. Both quantities are now fixed: the interaction parameter is constrained by gauge sector studies, as described in Appendix A, and the quark current mass delivers a realistic pion mass. Consequently, as in Refs. [17–19], all calculations herein are parameter-free.

3.2 Three-body interaction current

With the Poincaré-covariant nucleon wave function in hand, the nucleon gravitational form factors may be obtained from an interaction current constructed according to the scheme explained in Ref. [56]. That approach yields the current depicted in Fig. 2.

The diagrams in Fig. 2 are those which are necessary and sufficient to deliver symmetry-preserving results for the nonzero observable gravitational form factors of a nucleon described by the solution of the Faddeev equation in Fig. 1. One contribution is not drawn; namely, the nucleon analogue of the lower-panel in Ref. [19, Fig. 1]. This purely Q-longitudinal part of the probe + nucleon current need not be specified explicitly because it is entirely decoupled from the nonzero measurable form factors. Its role is analogous to Ref. [57, Fig. 3B′], which restores momentum conservation in calculations of pion DFs. Here, it provides for current conservation by ensuring

$$0 \equiv \bar{c}(Q^2) = \sum_{a = \substack{\text{dressed} \\ \text{quarks}}} \bar{c}^a(Q^2; \zeta_{\mathcal{H}}) =: \bar{c}^q(Q^2; \zeta_{\mathcal{H}}) . \tag{5}$$

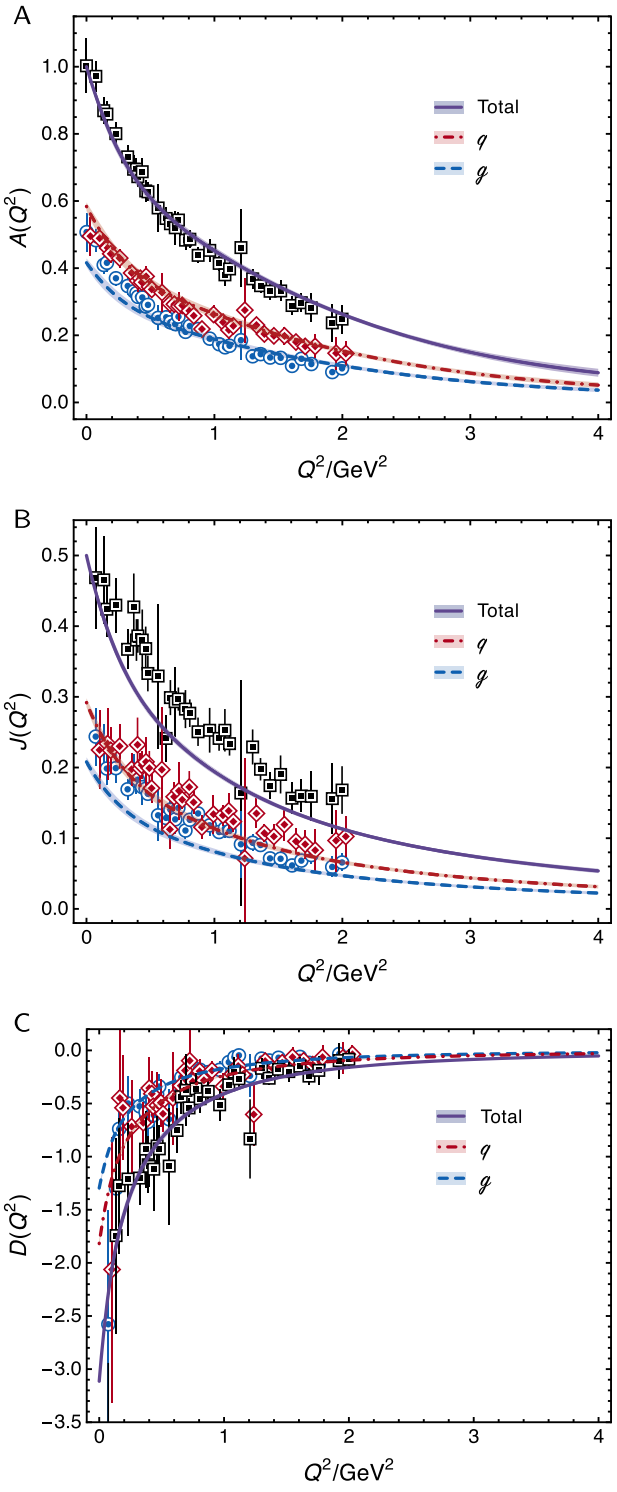

Fig. 3 Nucleon gravitational form factors. Curves – predictions herein: bracketing bands mark the extent of 1σ SPM uncertainty – see Appendix C for details. In each case, the overall (species-summed) result is independent of resolving scale, ζ. The species decompositions evolve with ζ. The lQCD points in each panel are reproduced from Ref. [24]: black squares – total form factor; blue circles – glue component; red diamonds – quark

The current in Fig. 2 involves the graviton + quark vertex, $\Gamma^g_{\mu\nu}$, a practicable solution for which was delivered in Ref. [19]. Amongst other things, Ref. [19] highlighted that, at low momentum transfers, graviton + hadron couplings receive contributions from the lightest tensor and scalar mesons in relevant channels, just as hadron electromagnetic form factors at low momenta are sensitive to the properties of the lightest neutral vector meson in a given quark + antiquark channel. We follow Ref. [19] in calculating $\Gamma^g_{\mu\nu}$. The results used herein are supplied in Appendix B.

4 Gravitational form factors: predictions

Our predictions for nucleon gravitational form factors are drawn in Fig. 3. The calculational procedure is now well established; nevertheless, for completeness, technical details are provided in Appendix C, which includes an explanation of the Schlessinger point method (SPM) used for interpolation and extrapolation of analytic functions [58–61].

The symmetry preserving character of our analysis is evident in the values of $A(0)$, $J(0)$ – see also Table 1. Notably, in delivering $J(0) = 1/2$, we confirm that the anomalous gravitomagnetic moment of a spin-1/2 system is zero [62–64]. Furthermore, the value of the nucleon "D-term", *viz.* $D(0) = -3.11(1)$ is a prediction.

A species decomposition of the observable nonzero form factors is enabled by the all-orders (AO) evolution scheme detailed in Ref. [65]. Here we list its key tenets. (*a*) There is an effective charge, $\alpha_{1\ell}(k^2)$, in the sense of Refs. [66,67] and reviewed in Ref. [42], that, when used to integrate the leading-order perturbative DGLAP equations [68–71], defines an evolution scheme for *every* parton distribution function (DF) that is all-orders exact. The pointwise form of $\alpha_{1\ell}(k^2)$ is largely irrelevant. Nevertheless, the process-independent strong running coupling defined and computed in Ref. [8] has all requisite properties. (*b*) There is a scale, $\zeta_{\mathcal{H}}$, at which all properties of a given hadron are carried by its valence degrees-of-freedom. At this scale, DFs associated with glue and sea quarks are zero. Working with the charge discussed in Refs. [8,42,43], the value of the hadron scale is a prediction [72]: $\zeta_{\mathcal{H}} = 0.331(2)$ GeV. Analysis of lQCD results relating to the pion valence quark DF yields a consistent result [38]: $\zeta_{\mathcal{H}} = 0.350(44)$ GeV.

Now consider a hadron H, some associated observable form factor $F(Q^2)$, and suppose one desires to reveal the contribution to $F(Q^2)$ from a parton species p at resolving scale ζ. Using AO evolution, then for any quark or gluon sector contributions, $F^q(Q^2;\zeta)$, $F^g(Q^2;\zeta)$, respectively, which are expressed in terms of the first/zeroth Mellin moment of some combination of generalised parton distributions (GPDs) at zero skewness, $\xi = 0$, the desired fractional

Table 1 $Q^2 = 0$ values of proton gravitational form factors plus species decompositions at $\zeta = \zeta_2 = 2$ GeV. Our analysis enables a separation of light-quark valence (V) and sea (S) components and expresses a charm (c) quark sea contribution. *N.B.* Uncertainties on sea and glue components are typically anticorrelated with those on the valence components. Such correlations are indicated by $\pm, \mp$. lQCD results reproduced from Ref. [24]: valence and sea are unseparated and no signal is reported for a c contribution. In both panels, q is the sum over all quark contributions, valence and sea

herein	$A(0)$	$J(0)$	$-D(0)$
Total	1.00	0.50	$3.114(10)_{\pm}$
u_V	$0.328(15)_{\pm}$	$0.164(08)_{\pm}$	$1.019(49)_{\pm}$
d_V	$0.149(07)_{\pm}$	$0.074(04)_{\pm}$	$0.463(22)_{\pm}$
u_S	$0.033(03)_{\mp}$	$0.017(02)_{\mp}$	$0.103(08)_{\mp}$
d_S	$0.042(03)_{\mp}$	$0.021(02)_{\mp}$	$0.131(11)_{\mp}$
s	$0.025(02)_{\mp}$	$0.012(02)_{\mp}$	$0.077(06)_{\mp}$
c	$0.0086(05)_{\mp}$	$0.0043(03)_{\mp}$	$0.027(02)_{\mp}$
q	$0.584(13)_{\pm}$	$0.292(06)_{\pm}$	$1.820(43)_{\pm}$
g	$0.416(13)_{\mp}$	$0.208(06)_{\mp}$	$1.294(33)_{\mp}$
lQCD	$A(0)$	$J(0)$	$-D(0)$
Total	1.011(37)	0.506(25)	3.87(97)
u	0.3255(92)	0.2213(85)	0.56(17)
d	0.1590(92)	0.0197(85)	0.57(17)
s	0.0257(95)	0.0097(82)	0.18(17)
q	0.510(25)	0.251(21)	1.30(49)
g	0.501(27)	0.255(13)	2.57(84)

contribution is [75, Secs. VII, VIII]:

$$F^p(Q^2;\zeta) = \langle x\rangle_\zeta^p \, F(Q^2)\,, \tag{6}$$

where $\langle x\rangle_\zeta^p$ is the parton species light-front momentum fraction in H at ζ. The nucleon gravitational form factors $A(Q^2)$, $J(Q^2)$ are in this class [25]. Following Ref. [76, Secs. 3.6-3.9], the AO scheme can be extended to obtain the same result for $D(Q^2)$. Thus, the species decompositions of all form factors in the gravitational current emerge and evolve in the same way. Exploiting these features, we arrive at the $\zeta = \zeta_2 := 2\,\text{GeV}$ species decompositions drawn in Fig. 3 and listed in Table 1.

The form factor $\bar{c}(Q^2)$, eliminated from Eq. (1) by current conservation, can also be decomposed into a sum over species contributions [25]. Considering such, we recall that dressed-quark contributions saturate all observable form factors at $\zeta_{\mathcal{H}}$; current construction, Eq. (5), entails $\bar{c}^q(Q^2;\zeta_{\mathcal{H}}) \equiv 0$; hence, $\bar{c}_g(Q^2;\zeta_{\mathcal{H}}) \equiv 0$. So, under AO evolution, following these arguments, each species contribution to $\bar{c}(Q^2)$ is zero at all scales: $\langle x\rangle_\zeta^p \times [\bar{c}(Q^2) \equiv 0] = 0$. Simplicity makes this an appealing explanation for $\bar{c}(Q^2) \equiv 0$, *viz.* at all scales, each species contribution to the current is separately conserved. Future analyses will see this notion confirmed or improved. Subsequently, alike with Ref. [24], we explore its consequences.

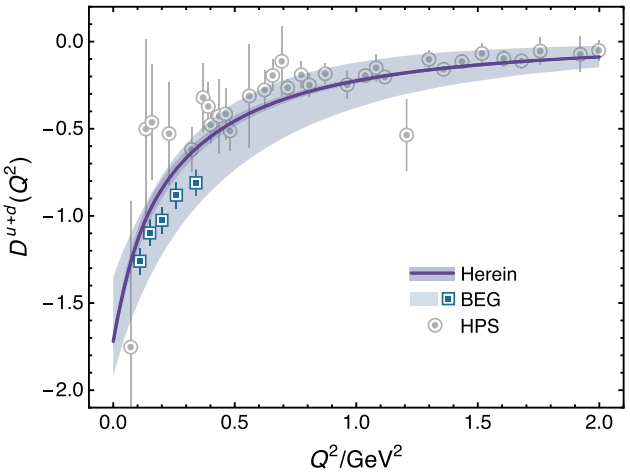

Fig. 4 Light-quark contribution to the proton D-term: $D^{u+d}(Q^2;\zeta)$. Herein – $D^{u+d}(Q^2;\zeta_2)$, solid purple curve within like-coloured 1σ SPM uncertainty band. BEG – squares and associated fit from Ref. [21], identified with the scale $\zeta \approx \zeta_{\text{B}} = 1.6\,\text{GeV}$ [73,74]. Circles – lQCD results from Ref. [24], obtained with $\zeta = \zeta_2$. Scale evolution is logarithmic; consequently, our predictions for $D^{u+d}(Q^2;\zeta_{\text{B}})$ and $D^{u+d}(Q^2;\zeta_2)$ are practically indistinguishable within line widths

Returning to the pressure form factor, considering light quarks alone, an inference from available data yields [21]: $D^{u+d}(0) = -1.63(29)$. This result may be identified with the scale $\zeta \approx \zeta_{\text{B}} = 1.6\,\text{GeV}$ [73,74]. Our study delivers $D^{u+d}(0;\zeta_{\text{B}}) = -1.79(5)$ and $D^{u+d}(0;\zeta_2) = -1.73(5)$. Notably, moreover, within uncertainties, our predictions are in Q^2 pointwise agreement with the extraction in Ref. [21] – see Fig. 4. As noted there, ζ-evolution is logarithmic; so, practically, within line widths, $D^{u+d}(Q^2;\zeta_{\text{B}}) = D^{u+d}(Q^2;\zeta_2)$.

Figure 3 also compares our predictions for the species separated form factors with available lQCD results: in all cases, they agree within mutual uncertainties.

One may quantify the preceding statement by noting that, for each form factor, the AO approach predicts that the contribution ratio gluon:total-quark is a fixed number (constant, independent of Q^2), *viz.*

$$F = A, J, D \;|\; \frac{F^g(Q^2;\zeta_2)}{\sum_q F^q(Q^2;\zeta_2)} = 0.71(4)\,. \tag{7}$$

(The value grows with ζ.) Regarding Fig. 5, it is apparent that, within their (large) uncertainties, available lQCD results are compatible with Eq. (7). Namely, for each form factor, the lQCD results are (a) consistent with a Q^2-independent ratio of glue-to-quark contributions and (b) a value of this ratio that matches our prediction. This is true when one considers the combination of all form factors, Fig. 5 A, in which the lQCD result is $g/q = 0.82(18)$, where the uncertainty marks 1σ

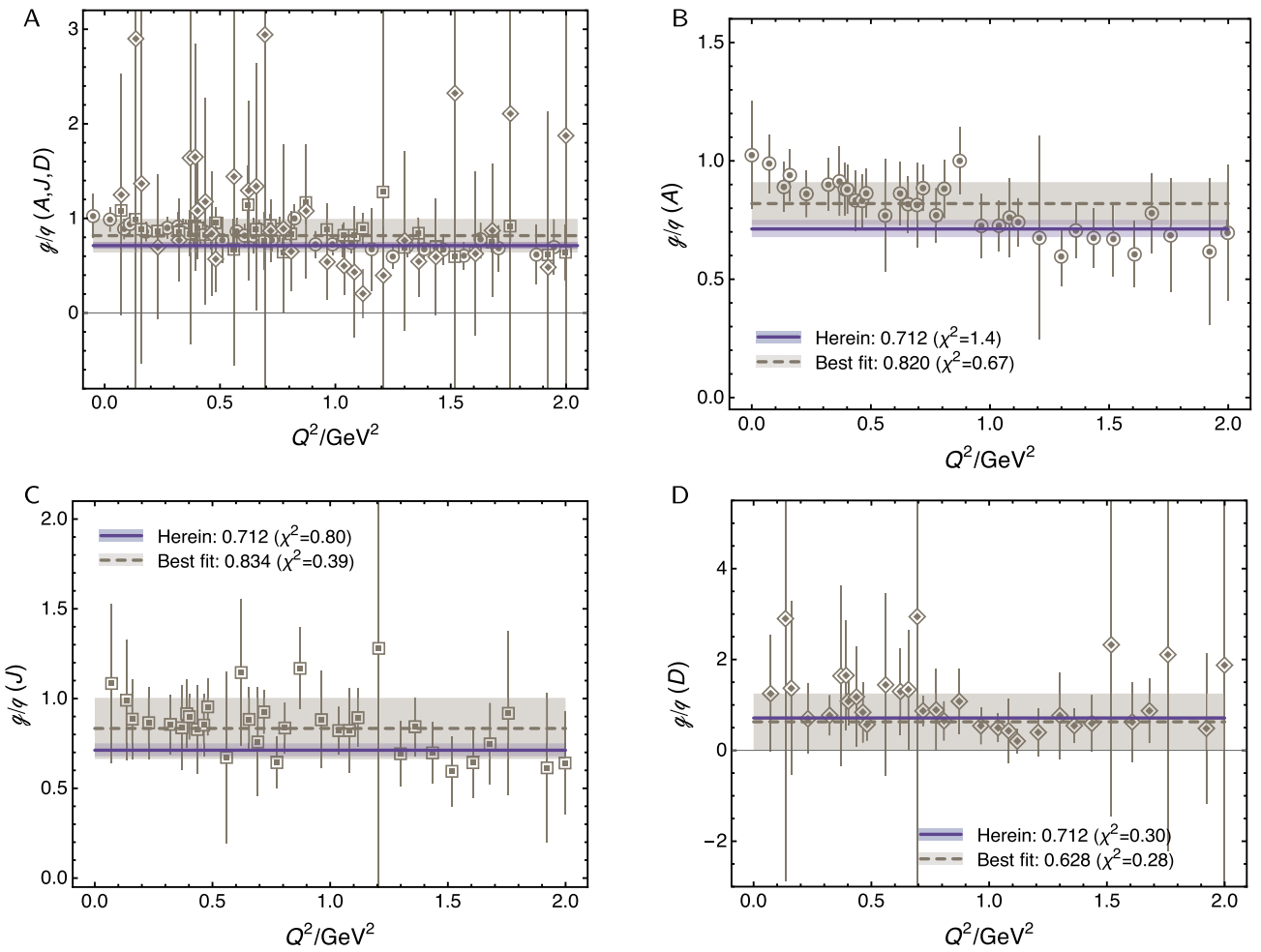

Fig. 5 Panel A. Combined A, J, D lQCD g/q results (grey points): grey line – uncertainty weighted average of all points; and grey band – 1σ around the central value: 0.82(18). Panels B, C, D. lQCD results for individual gravitational form factors: grey line – uncertainty weighted average in each case along with 1σ grey band, as specified in each panel. Prediction herein: $g/q = 0.71(4)$ (purple line and band) – all panels. Resolving scale: $\zeta = \zeta_2$

about the central value, and also the individual form factors – see Fig. 5 B–D.

Comparison of the panels in Table 1 yields additional insights.

(*a*) Considering the light-quark $Q^2 = 0$ contributions, our predictions are in the ratio $u/d = 1.9$ for all form factors. On the other hand, the lQCD results are: $A = 2.05(13)$; $J = 11.2(4.5)$; $D = 0.98(42)$. Evidently, whilst the lQCD form factor with the smallest uncertainty, A, yields a ratio consistent with our prediction, the other two, with larger uncertainties, disagree greatly.

(*b*) Regarding $A^g(0)$, unlike the lQCD result [24], our prediction matches the value inferred from global analyses of data by many collaborations [77]: $A^g(0) = 0.413(6)$.

(*c*) Our predicted values for both the quark and gluon contributions to $J(0)$ (proton spin) align with those reported in Refs. [39,78] (quark + diquark picture of the nucleon) and also match the lQCD results reported in Ref. [79]. They differ from those in Ref. [24]: most notably, herein and in Refs. [39,78,79], the quark contribution is greater than the glue contribution, whereas there is a signal for this being reversed in Ref. [24].

(*d*) We find that the glue contribution to $D(0)$ is noticeably smaller than the quark contribution, with a ratio 0.71(4) – Eq. (7). On the other hand, Ref. [24] reports a different result, with glue markedly greater than quark: 1.97(65), albeit with large uncertainty.

5 Density profiles

Working with the Poincaré-invariant nucleon gravitational form factors obtained herein, one may calculate an array of

Breit frame density profiles (energy, pressure, shear and normal force distributions) via appropriate three-dimensional Fourier transforms [25]. The relevant formulae are collected in Appendix D. Questions concerning the interpretation of such distributions have been widely canvassed – see, *e.g.*, Refs. [80–84]. Other transforms are possible [84]. Nevertheless, since the input function in any case is always the same, then no projective mapping, like the construction of a density in two or three spacelike dimensions, can deliver any objective information that is not already contained in the Poincaré-invariant subject function. Thus, whatever type of transform is chosen, it is merely a mathematical operation on the same input object; hence, interpreted judiciously, all outputs are qualitatively equivalent.

Figure 6 displays the predictions for the nucleon pressure and shear force distributions in comparison with those in the pion, calculated using the same framework [19]. Evidently, the pion peak values are roughly twice those in the proton. It is here worth reiterating [19,21] that such pressures are an order of magnitude greater than are expected at the core of neutron stars [85].

It is worth discussing nucleon mass and mechanical radii. The former is determined by $A(Q^2)$, $D(Q^2)$ and the latter by $D(Q^2)$ alone – see Eq. (D.16b):

$$r_{\rm mass} = 0.81(5) r_{\rm ch}\,, \quad r_{\rm mech} = 0.72(2) r_{\rm ch}\,, \tag{8}$$

where $r_{\rm ch} = 0.887(3)$ fm is the proton charge radius calculated using the same framework [18]. Regarding species decompositions, at ζ_2:

$$r^q_{\rm mass} = 0.62(4) r_{\rm ch}\,, \; r^g_{\rm mass} = 0.52(3) r_{\rm ch}\,, \tag{9a}$$
$$r^q_{\rm mech} = 0.55(2) r_{\rm ch}\,, \; r^g_{\rm mech} = 0.47(2) r_{\rm ch}\,. \tag{9b}$$

Reviewing these predictions, we are led to stress the following points.

(a) The analysis herein is the only one available that provides a unified single-framework (phenomenological or theoretical) treatment of nucleon electromagnetic and gravitational form factors. This makes the relative radii ordering statements unique and substantive.
(b) The nucleon's mechanical radius is less than its mass radius. On the other hand, the available lQCD comparison suggests the reverse ordering, although the two radii are equal within lQCD uncertainties.
(c) Alike with the pion [86], the proton's mass radius is less than its charge radius.
(d) Regarding species separated radii at ζ_2, we predict the quark contribution is greater than that from glue. The reverse ordering is favoured in Ref. [24]. In our view, considering Table 1 and the associated discussion, this owes largely to the lQCD overestimate of the glue contribution to $D(Q^2)$.
(e) Within uncertainties, our prediction for the quark pressure, Fig. 6A, matches that inferred from data [21]. Likewise, our result for $r_{\rm mech}$ matches that inferred therein.
(f) Considering the discussion in Refs. [87–92], comparisons with currently reported inferences of glue contributions to proton gravitational form factors are unwarranted.

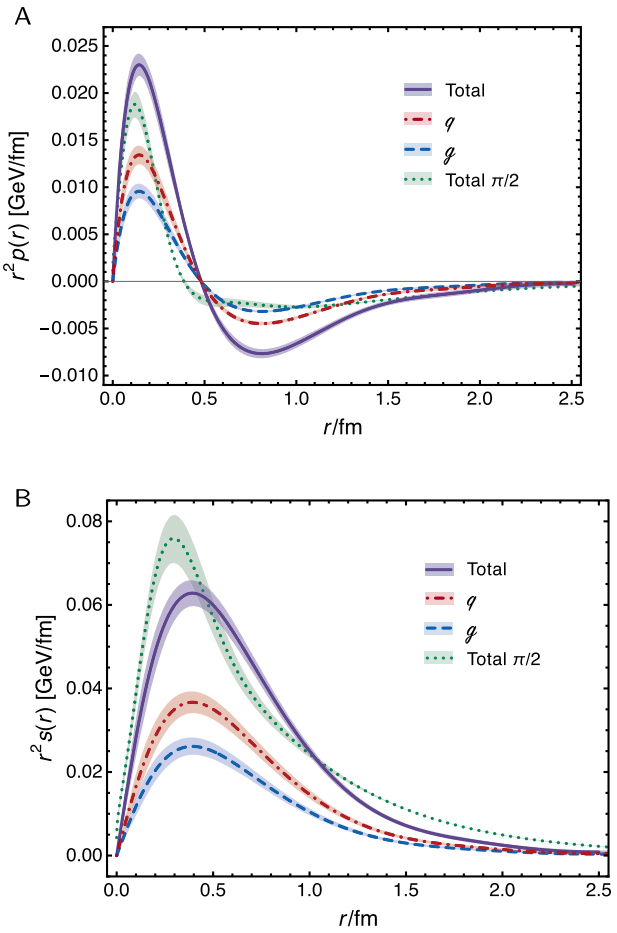

Fig. 6 Nucleon pressure, $p(r)$, and shear force, $s(r)$, distributions, along with total-quark and glue species decompositions at ζ_2. Like pion distributions are drawn in green. *N.B.* The pion distributions are divided by 2. In all cases, the like-coloured band marks the extent of 1σ SPM uncertainty

6 Summary

Using a symmetry-preserving, systematically-improvable truncation of the quantum field equations relevant to calculation of hadron properties, this study completes the first single-framework, unifying treatment of pion, kaon, nucleon electromagnetic and gravitational form factors. Each element

in the study is a well-defined approximation to an analogous quantity in quantum chromodynamics (QCD). A single parameter characterises the quark + quark scattering kernel. It is fixed with reference to gauge sector dynamics in QCD; so, all predictions are parameter-free and link observables directly with the three pillars of emergent hadron mass.

Amongst other things, the analysis reveals the following features. Regarding a separation of each of the nucleon's gravitational form factors (mass, spin, D-term) into glue and quark pieces, the ratio of these contributions is the same Q^2-independent number for all three: glue/quark ≈ 0.71. This novel algebraic prediction is consistent with available results from the numerical simulation of lattice-regularised QCD (lQCD). The near-core pressure in the pion is roughly twice that in the proton, so both are at least an order of magnitude greater than that of a neutron star. The nucleon's mechanical radius is less than its mass radius, which in turn is less than its charge radius. At a standard resolving scale, $\zeta = 2\,\text{GeV}$, the glue contributions to both are 15% less than the total quark contributions. Within uncertainties, our predictions are consistent with phenomenological inferences from available data on deeply virtual Compton scattering.

No improvement on the analysis herein can be anticipated before simulations of lQCD have simultaneously delivered infinite-volume, continuum-limit, carefully renormalised, realistic pion mass studies of all physical properties discussed above, *viz.* pion, kaon, nucleon electromagnetic and gravitational form factors. Meanwhile, the breadths of application and success of the parameter-free framework we have employed suggest that the predictions delivered should serve as benchmarks for future phenomenology and theory in an era that will see completion of high-luminosity, high-energy accelerators that promise to be able to test them.

Acknowledgements We are grateful for constructive interactions with S.-X. Qin. Work supported by: National Natural Science Foundation of China (grant nos. 12135007, 12233002); Natural Science Foundation of Jiangsu Province (grant no. BK20220122); Spanish Ministry of Science and Innovation (MICINN grant no. PID2022-140440NB-C22); and Junta de Andalucía (grant no. P18-FR-5057).

Data Availibility Statement Data will be made available on reasonable request. [Authors' comment: All information necessary to reproduce the results described herein is contained in the material presented above.]

Code Availability Statement Code/software will be made available on reasonable request. [Authors' comment: No additional remarks.]

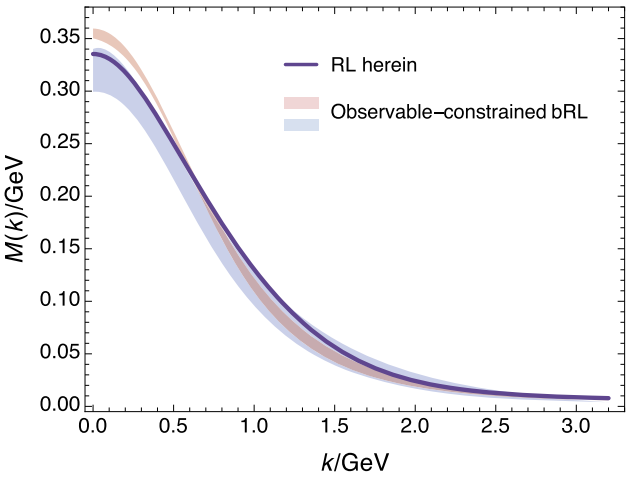

Fig. 7 Dressed light quark mass function: $M(k) = B(k)/A(k)$ – see Eq. (2). Solid purple curve – RL result calculated and used herein to deliver all predictions. Blue and red bands – range of results admitted by the observable-constrained, nonperturbative beyond-RL (bRL) truncation described in Ref. [34]

Appendix A Quark + Quark Interaction

A context for the interaction in Eq. (4) is provided by noting that, following Ref. [51], one may draw a connection between $\tilde{\mathcal{G}}$ and QCD's process-independent effective charge, discussed in Refs. [8,42,43]. That effective charge is characterised by an infrared coupling value $\hat{\alpha}(0)/\pi = 0.97(4)$ and a gluon mass-scale $\hat{m}_0 = 0.43(1)\,\text{GeV}$ determined in a combined continuum and lattice analysis of QCD's gauge sector [8]. The following values are those of analogous quantities inferred from Eq. (2):

$$\alpha_{\mathcal{G}}(0)/\pi = 1.45\,, \quad m_{\mathcal{G}} = 0.54\,\text{GeV}\,. \tag{A.1}$$

They are a fair match with the QCD values, especially since earlier, less well informed versions of the RL interaction yielded $\alpha_{\mathcal{G}}(0)/\pi \approx 15$, *i.e.*, a value ten-times larger [51].

Existing analyses of hadron properties suggest that inclusion of corrections to RL truncation in ground state channels has little impact beyond a relaxation of the numbers in Eq. (A.1) toward their QCD values; for instance, compare the RL and EHM-improved spectra in Ref. [35]. This is further highlighted by Fig. 7, which displays the mass function used herein to deliver the nucleon gravitational form factors. Obtained by solving the quark gap equation with the RL kernel specified by Eqs. (3), (4), it falls comfortably within the solution range determined by solving the gap equation with

the symmetry-preserving, nonperturbative beyond-RL truncation described in Ref. [34]. It is for these reasons that the modern formulation of RL truncation provides a reliable, predictive tool – see also, *e.g.*, Refs. [17,18], in which it was used to deliver pion, kaon, and nucleon electromagnetic form factors, and Ref. [19], wherein pion and kaon gravitational form factors are calculated.

Appendix B Quark + graviton vertex

Here we briefly review the analysis in Ref. [19] – those seeking details may refer therein.

The dressed graviton + quark vertex satisfies the following Ward–Green–Takahashi (WGT) identity:

$$Q_\mu i\Gamma^g_{\mu\nu}(k,Q) = S^{-1}(k_+)k_{-\nu} - S^{-1}(k_-)k_{+\nu}. \tag{B.2}$$

In RL truncation, $\Gamma^g_{\mu\nu}$ is obtained by solving the following inhomogeneous Bethe-Salpeter equation:

$$\begin{aligned} i\Gamma^g_{\mu\nu}(k_+,k_-) &= Z_2[i\gamma_\mu k_\nu - \delta_{\mu\nu}(i\gamma\cdot k + Z_m^0 m^\zeta)] \\ &\quad + Z_2^2\int_{dl}^{\Lambda} \mathcal{K}(k-l)[S(l_+)i\Gamma^g_{\mu\nu}(l_+,l_-)S(l_-)]\,, \end{aligned} \tag{B.3}$$

where $k_\pm = k \pm Q/2$, Z_m^0 is the chiral-limit mass renormalisation constant, and Z_2 is the quark wave function renormalisation constant. (In all analyses discussed herein, a mass-independent momentum-subtraction renormalisation scheme is employed [93].)

With complete generality, the solution of Eq. (B.3) may be written thus:

$$\Gamma^g_{\mu\nu}(k,Q) = \Gamma^{gM}_{\mu\nu}(k,Q) + \Gamma^{gT}_{\mu\nu}(k,Q). \tag{B.4}$$

The first term:

$$\begin{aligned} &i\Gamma^{gM}_{\mu\nu}(k,Q) \\ &\quad = i\Gamma^{\rm BC}_\mu(k,Q)k_\nu - \tfrac{1}{2}\delta_{\mu\nu}[S^{-1}(k_+) + S^{-1}(k_-)] \\ &\qquad + iT_{\mu\alpha}(Q)T_{\nu\beta}(Q)4\hat{\Gamma}^2_{\alpha\beta}(k_+,k_-), \end{aligned} \tag{B.5}$$

with

$$i\Gamma^{\rm BC}_\nu(k_+,k_-) = i\gamma_\nu\Sigma_{A_\pm} + 2ik_\nu\gamma\cdot k\,\Delta_{A_\pm} + 2k_\nu\Delta_{B_\pm}, \tag{B.6}$$

$\Sigma_{A_\pm} = [A(k_+^2)+A(k_-^2)]/2, \Delta_{F_\pm} = [F(k_+^2)-F(k_-^2)]/[k_+^2 - k_-^2]$, $F = A, B$, resolves Eq. (B.2).

$\Gamma^2_{\alpha\beta}(k;Q)$ in Eq. (B.5) is the tensor + quark vertex generated by the inhomogeneity

$$\Gamma^2_{0\mu\nu}(k;Q) = T_{\mu\alpha}(Q)T_{\nu\beta}(Q)\tfrac{1}{2}\left(\gamma_\alpha k_\beta + \gamma_\beta k_\alpha\right), \tag{B.7}$$

with $\hat{\Gamma}(k,Q) = \Gamma(k,Q) - \Gamma(k,0)$ so as to ensure the absence of kinematic singularities. Dynamical singularities nevertheless appear in $\Gamma^2_{\mu\nu}$; namely, one at the pole position of each $I = 0$ tensor meson. Since $\Gamma^2_{\mu\nu}$ possesses eight independent Dirac matrix valued tensor structures, then Eq. (B.5) involves thirteen such nonzero terms.

The remaining piece in Eq. (B.4), $\Gamma^{gT}_{\mu\nu}(k,Q)$, satisfies $Q_\mu\Gamma^{gT}_{\mu\nu}(k,Q) = 0$. It represents all possible transverse structures not already included in the first term. Like $\Gamma^2_{\mu\nu}$, $\Gamma^{gT}_{\mu\nu}$ does not contribute to resolving Eq. (B.2). It is obtained by solving the appropriate Bethe-Salpeter equation. In doing so, one sees the emergence of isoscalar scalar mesons in the graviton + quark vertex.

As stressed in Ref. [19], a few contributions dominate the graviton + light-quark vertex, *viz.* those parts which saturate the WGT identity – already included; pieces associated with an f_2 tensor meson pole – incorporated via $\Gamma^2_{\alpha\beta}(k;Q)$; and those tied to an analogous scalar meson resonance. The last is captured by writing

$$\Gamma^{gT}_{\mu\nu}(k,Q) = T_{\mu\nu}(Q)\Gamma_{\mathbb{I}}(k;Q)\,, \tag{B.8}$$

where $\Gamma_{\mathbb{I}}(k;Q)$, which has four independent Dirac matrix valued structures, $D_{\mathbb{I}}^{j=1,4} \propto \{\mathbf{1}, \gamma\cdot k, \gamma\cdot Q, \sigma_{\alpha\beta}k_\alpha Q_\beta\}$ – see, *e.g.*, Ref. [94, Appendix A], is obtained by solving

$$\begin{aligned} &{\rm tr}_D\mathcal{P}^j_{\mu\nu}(k,Q)\Gamma^{gT}_{\mu\nu}(k_+k_-) \\ &\quad = {\rm tr}_D\mathcal{P}^j_{\mu\nu}(k,Q)Z_2^2\int_{dl}^{\Lambda}\mathcal{K}(k-l)S(l_+) \\ &\qquad \times\{\Gamma^{gM}_{\mu\nu}(l_+,l_-) + T_{\mu\nu}(Q)\Gamma_{\mathbb{I}}(l_+;l_-)\}S(l_-)\,. \end{aligned} \tag{B.9}$$

Here,

$${\rm tr}\mathcal{P}^j_{\mu\nu}(k,Q)\Gamma^{gT}_{\mu\nu}(k,Q) = D^j_{\mathbb{I}}, \tag{B.10a}$$

$${\rm tr}\mathcal{P}^j_{\mu\nu}(k,Q)\Gamma^{gM}_{\mu\nu}(k,Q) \equiv 0\,. \tag{B.10b}$$

At this point, gathering all terms described above, one has an efficacious solution for the graviton + quark vertex. It involves 2 one-variable and 12 two-variable functions and various distinct, associated Dirac matrix structures. For completeness, we list results for the lightest scalar ($\mathbb{S}$) and tensor ($\mathbb{T}$) mesons, *viz.* the calculated masses and residue coefficients (in GeV):

	$m_{\mathbb{S}}$	$f_{\mathbb{S}}$	$m_{\mathbb{T}}$	$f_{\mathbb{T}}$
$u=d$	0.53	0.025	1.20	0.042

. (B.11)

Appendix C Form factors and SPM

The Faddeev amplitude depends on the nucleon total momentum, P, and two relative momenta, p, q; so each function in the amplitude depends on three angular variables defined via the inner products $p \cdot q$, $p \cdot P$, $q \cdot P$. In solving the Faddeev equation, we used eight Chebyshev polynomials to express the dependence on each angle [49]. This enables evaluation of Ψ at any required integration point in either the Faddeev equation or the current. P is a complex-valued (timelike) vector, $P^2 = -m_N^2$, whereas Q is spacelike. Thus, when evaluating the current, the integrand sample points are typically in the complex plane and the integrand exhibits oscillations whose amplitudes grow with Q^2 [95]. To handle this, increasing the number of Chebyshev polynomials and quadrature points is effective on $Q^2 \leq Q^2_{\rm m}$, $Q^2_{\rm m} \approx 2.5\,{\rm GeV}^2$. At larger Q^2 values, however, such a brute force approach fails to deliver accurate results. (Regarding nucleon electromagnetic form factors, where $\Gamma^g_{\mu\nu}$ is replaced by the simpler photon + quark vertex, direct reach to larger Q^2 is possible [18].)

To obtain results on $Q^2 \gtrsim 2.5\,{\rm GeV}^2$, we extrapolate using the Schlessinger point method (SPM) [58–60]. The SPM is grounded in analytic function theory and based on the Padé approximant. It accurately reconstructs any function in the complex plane within a radius of convergence determined by that one of the function's branch points which lies closest to the real domain that provides the sample points. Modern implementations introduce a statistical element; so, the extrapolations come with an objective and reliable quantitative estimate of uncertainty. Crucially, the SPM is free from practitioner-induced bias; so, delivers objective analytic continuations. In practice, the SPM has been blind-tested against numerous models and physically validated in applications that include determination of hadron and light nucleus radii from electron scattering [96]; extraction of resonance properties from scattering data [97]; searching for evidence of the odderon in high-energy elastic hadron+hadron scattering [98]; and calculation of meson and baryon electromagnetic form factors [17,18].

Our SPM extrapolations are developed as follows.

Step 1 For each form factor, we produce $N = 30$ directly calculated values of $Q^2\times$ form factor, spaced evenly on $Q^2 \lesssim 2.5\,{\rm GeV}^2$.

Step 2 From that set, $M_0 = 6$ points are chosen at random, the usual SPM continued fraction interpolation is constructed, and that function is extrapolated onto $Q^2 > Q^2_{\rm m}$. The curve is retained so long as it is singularity free on $Q^2 \leq 100\,{\rm GeV}^2$.

Step 3 Step 2 is repeated with another set of M_0 randomly chosen points.

Step 4 One continues with 2 and 3 until $n_{M_0} = 200$ smooth extrapolations are obtained.

Step 5 Steps 2 and 3 are repeated for $M = \{M_0 + 2i | i = 1, \ldots, 5\}$.

Step 6 At this point, one has 1 200 statistically independent extrapolations for $Q^2\times$ form factor.

Working with these extrapolations, then at each value of Q^2, we record the mean value of all curves as the central prediction and report as the uncertainty the function range which contains 68% of all the extrapolations – this is a 1σ band.

Appendix D Breit frame density profiles

Energy, pressure, and shear force distributions have been defined via the following formulae [25] ($t = Q^2$):

$$\epsilon(r) = m_N \left(\hat{A}(r) - \tfrac{1}{4m_N^2} \left[\widehat{(tD)}(r) + \widehat{(tA)}(r) - 2\widehat{(tJ)}(r) \right] \right), \tag{D.12a}$$

$$p(r) = \frac{1}{6m_N} \frac{1}{r^2} \frac{d}{dr} r^2 \frac{d}{dr} \hat{D}(r)\,, \tag{D.12b}$$

$$s(r) = -\frac{1}{4m_N} r \frac{d}{dr} \frac{1}{r} \frac{d}{dr} \hat{D}(r)\,, \tag{D.12c}$$

which involve the Fourier transform

$$\hat{f}(|\vec{r}|) = \int \frac{d^3q}{(2\pi)^3} {\rm e}^{\vec{q}\cdot\vec{r}} f(t \to |\vec{q}|^2)\,. \tag{D.13}$$

Species decompositions may be obtained by replacing each total form factor by its species component – recall Eq. (5) and associated discussions.

In terms of the quantities just defined, the normal force distribution in the nucleon is

$$F^{\|}(r) = p(r) + (2/3)s(r)\,. \tag{D.14}$$

Nucleon mass and mechanical radii can now be defined in terms of $\epsilon(r)$, $F^{\|}(r)$ [25]:

$$\langle r^2 \rangle_{\rm mass} = \frac{\int d^3r\, r^2 \epsilon(r)}{\int d^3r \epsilon(r)}\,, \tag{D.15a}$$

$$\langle r^2 \rangle_{\rm mech} = \frac{\int d^3r\, r^2 F^{\|}(r)}{\int d^3r\, F^{\|}(r)}\,. \tag{D.15b}$$

In a common interpretation, the mechanical radius measures the extent of the nucleon's normal force distribution. These expressions are equivalent to the following, which are typi-

cally easier to use:

$$\langle r^2\rangle_{\rm mass} = \left[-6\frac{d}{dt}A(t)\Big|_{t=0} - 3\frac{D(0)}{2m_N^2}\right]\frac{1}{A(0)}\,, \tag{D.16a}$$

$$\langle r^2\rangle_{\rm mech} = \frac{6}{\int_0^\infty dt\,[D(t)/D(0)]}\,. \tag{D.16b}$$

Consider Eq. (D.16a).

(*a*) Making the replacements $A \to F_1$, $D \to -F_2$, where $F_{1,2}$ are nucleon Dirac and Pauli electromagnetic form factors, then this formula is mapped into that for the nucleon charge radius, $r_{\rm ch}^2$. Consequently, a $r_{\rm mass}$:$r_{\rm ch}$ comparison is natural.

(*b*) Regarding the total mass form factor, $A(0) = 1$; but this is not true for species separated contributions. Notwithstanding that, under AO evolution, individual species contributions to a given radius are simply determined by their light-front momentum fractions at the associated scale. This is plain from Sect. 3.1 and Ref. [75, Sec. VIII.B].

(*c*) The second term in Eq. (D.16a) is large and positive: using our predictions, the value is $(0.45\,{\rm fm})^2$.

(*d*) A trace-anomaly form factor, $\theta(t)$, and associated density may be constructed [25] by making the replacement $tD(t) \to 3tD(t)$ in Eq. (D.12a). The associated radius-squared is

$$\langle r^2\rangle_\theta = \langle r^2\rangle_{\rm mass} - 3D(0)/m_N^2 > \langle r^2\rangle_{\rm mass}. \tag{D.17}$$

However, owing to the magnitude and sign of $D(t)$, $\theta(t)$ is not positive definite, something which diminishes its appeal as a mass distribution form factor [99, Fig. 4].

Regarding Eq. (D.16b), it is evident that the mechanical radius is determined solely by the integral of the $Q^2 = 0$ unit-normalised version of the nucleon D-term function.

References

1. C.D. Roberts, D.G. Richards, T. Horn, L. Chang, Insights into the emergence of mass from studies of pion and kaon structure. Prog. Part. Nucl. Phys. **120**, 103883 (2021)
2. D. Binosi, Emergent Hadron Mass in Strong Dynamics. Few Body Syst. **63**(2), 42 (2022)
3. M. Ding, C.D. Roberts, S.M. Schmidt, Emergence of Hadron Mass and Structure. Particles **6**(1), 57–120 (2023)
4. M.N. Ferreira, J. Papavassiliou, Gauge Sector Dynamics in QCD. Particles **6**(1), 312–363 (2023)
5. K. Raya, A. Bashir, D. Binosi, C.D. Roberts, J. Rodríguez-Quintero, Pseudoscalar Mesons and Emergent Mass. Few Body Syst. **65**(2), 60 (2024)
6. C.D. Roberts, A.G. Williams, Dyson-Schwinger equations and their application to hadronic physics. Prog. Part. Nucl. Phys. **33**, 477–575 (1994)
7. J.M. Cornwall, Dynamical Mass Generation in Continuum QCD. Phys. Rev. D **26**, 1453 (1982)
8. Z.-F. Cui, J.-L. Zhang, D. Binosi, F. de Soto, C. Mezrag, J. Papavassiliou, C.D. Roberts, J. Rodríguez-Quintero, J. Segovia, S. Zafeiropoulos, Effective charge from lattice QCD. Chin. Phys. C **44**, 083102 (2020)
9. K.D. Lane, Asymptotic Freedom and Goldstone Realization of Chiral Symmetry. Phys. Rev. D **10**, 2605 (1974)
10. H.D. Politzer, Effective Quark Masses in the Chiral Limit. Nucl. Phys. B **117**, 397 (1976)
11. M. Ablikim et al., Future Physics Programme of BESIII. Chin. Phys. C **44**(4), 040001 (2020)
12. D. P. Anderle, et al., Electron-ion collider in China, Front. Phys. (Beijing) 16 (6) (2021) 64701
13. J. Arrington et al., Revealing the structure of light pseudoscalar mesons at the electron–ion collider. J. Phys. G **48**, 075106 (2021)
14. C. Quintans, The New AMBER Experiment at the CERN SPS. Few Body Syst. **63**(4), 72 (2022)
15. D.S. Carman, R.W. Gothe, V.I. Mokeev, C.D. Roberts, Nucleon Resonance Electroexcitation Amplitudes and Emergent Hadron Mass. Particles **6**(1), 416–439 (2023)
16. V. I. Mokeev, P. Achenbach, V. D. Burkert, D. S. Carman, R. W. Gothe, A. N. Hiller Blin, E. L. Isupov, K. Joo, K. Neupane, A. Trivedi, First Results on Nucleon Resonance Electroexcitation Amplitudes from $ep \to e'\pi^+\pi^- p'$ Cross Sections at W = 1.4-1.7 GeV and Q^2 = 2.0-5.0 GeV^2, Phys. Rev. C 108 (2) (2023) 025204
17. Z.-Q. Yao, D. Binosi, C.D. Roberts, Onset of scaling violation in pion and kaon elastic electromagnetic form factors. Phys. Lett. B **855**, 138823 (2024)
18. Z.-Q. Yao, D. Binosi, Z.-F. Cui, C. D. Roberts, Nucleon charge and magnetisation distributions: flavour separation and zeroes. https://doi.org/10.1016/j.fmre.2024.11.005
19. Y.-Z. Xu, M. Ding, K. Raya, C.D. Roberts, J. Rodríguez-Quintero, S.M. Schmidt, Pion and kaon electromagnetic and gravitational form factors. Eur. Phys. J. C **84**(2), 191 (2024)
20. D.C. Hackett, P.R. Oare, D.A. Pefkou, P.E. Shanahan, Gravitational form factors of the pion from lattice QCD. Phys. Rev. D **108**(11), 114504 (2023)
21. V.D. Burkert, L. Elouadrhiri, F.-X. Girod, The pressure distribution inside the proton. Nature **557**(7705), 396–399 (2018)
22. K. Kumerički, Measurability of pressure inside the proton. Nature **570**(7759), E1–E2 (2019)
23. H. Moutarde, P. Sznajder, J. Wagner, Unbiased determination of DVCS Compton Form Factors. Eur. Phys. J. C **79**, 614 (2019)
24. D.C. Hackett, D.A. Pefkou, P.E. Shanahan, Gravitational Form Factors of the Proton from Lattice QCD. Phys. Rev. Lett. **132**(25), 251904 (2024)
25. M.V. Polyakov, P. Schweitzer, Forces inside hadrons: pressure, surface tension, mechanical radius, and all that. Int. J. Mod. Phys. A **33**(26), 1830025 (2018)
26. H.J. Munczek, Dynamical chiral symmetry breaking, Goldstone's theorem and the consistency of the Schwinger-Dyson and Bethe-Salpeter Equations. Phys. Rev. D **52**, 4736–4740 (1995)
27. A. Bender, C.D. Roberts, L. von Smekal, Goldstone Theorem and Diquark Confinement Beyond Rainbow- Ladder Approximation. Phys. Lett. B **380**, 7–12 (1996)
28. C.S. Fischer, R. Williams, Probing the gluon self-interaction in light mesons. Phys. Rev. Lett. **103**, 122001 (2009)
29. L. Chang, C.D. Roberts, Sketching the Bethe-Salpeter kernel. Phys. Rev. Lett. **103**, 081601 (2009)
30. L. Chang, I.C. Cloet, J.J. Cobos-Martinez, C.D. Roberts, S.M. Schmidt, P.C. Tandy, Imaging dynamical chiral symmetry break-

ing: pion wave function on the light front. Phys. Rev. Lett. **110**, 132001 (2013)
31. D. Binosi, L. Chang, J. Papavassiliou, C.D. Roberts, Bridging a gap between continuum-QCD and ab initio predictions of hadron observables. Phys. Lett. B **742**, 183–188 (2015)
32. R. Williams, C.S. Fischer, W. Heupel, Light mesons in QCD and unquenching effects from the 3PI effective action. Phys. Rev. D **93**, 034026 (2016)
33. D. Binosi, L. Chang, S.-X. Qin, J. Papavassiliou, C.D. Roberts, Symmetry preserving truncations of the gap and Bethe-Salpeter equations. Phys. Rev. D **93**, 096010 (2016)
34. D. Binosi, L. Chang, J. Papavassiliou, S.-X. Qin, C.D. Roberts, Natural constraints on the gluon-quark vertex. Phys. Rev. D **95**, 031501(R) (2017)
35. Z.-N. Xu, Z.-Q. Yao, S.-X. Qin, Z.-F. Cui, C.D. Roberts, Bethe-Salpeter kernel and properties of strange-quark mesons. Eur. Phys. J. A **59**(3), 39 (2023)
36. C. Chen, C.S. Fischer, C.D. Roberts, J. Segovia, Nucleon axial-vector and pseudoscalar form factors and PCAC relations. Phys. Rev. D **105**(9), 094022 (2022)
37. L. Chang, C.D. Roberts, Regarding the distribution of glue in the pion. Chin. Phys. Lett. **38**(8), 081101 (2021)
38. Y. Lu, Y.-Z. Xu, K. Raya, C.D. Roberts, J. Rodríguez-Quintero, Pion distribution functions from low-order Mellin moments. Phys. Lett. B **850**, 138534 (2024)
39. Y. Yu, P. Cheng, H.-Y. Xing, F. Gao, C.D. Roberts, Contact interaction study of proton parton distributions. Eur. Phys. J. C **84**(7), 739 (2024)
40. C. Chen, C.S. Fischer, C.D. Roberts, Nucleon to Δ axial and pseudoscalar transition form factors. Phys. Rev. Lett. **133**(13), 131901 (2024)
41. C. Alexandrou, et al., Quark and gluon momentum fractions in the pion and in the kaon. Phys. Rev. Lett. **134**(13), (2025). https://doi.org/10.1103/PhysRevLett.134.131902
42. A. Deur, S.J. Brodsky, C.D. Roberts, QCD Running Couplings and Effective Charges. Prog. Part. Nucl. Phys. **134**, 104081 (2024)
43. S.J. Brodsky, A. Deur, C.D. Roberts, The Secret to the Strongest Force in the Universe. Sci. Am. **5**(May), 32–39 (2024)
44. G. Eichmann, R. Alkofer, A. Krassnigg, D. Nicmorus, Nucleon mass from a covariant three-quark Faddeev equation. Phys. Rev. Lett. **104**, 201601 (2010)
45. S.-X. Qin, C.D. Roberts, S.M. Schmidt, Poincaré-covariant analysis of heavy-quark baryons. Phys. Rev. D **97**, 114017 (2018)
46. Q.-W. Wang, S.-X. Qin, C.D. Roberts, S.M. Schmidt, Proton tensor charges from a Poincaré-covariant Faddeev equation. Phys. Rev. D **98**, 054019 (2018)
47. S.-X. Qin, C.D. Roberts, S.M. Schmidt, Spectrum of light- and heavy-baryons. Few Body Syst. **60**, 26 (2019)
48. G. Eichmann, C.S. Fischer, Nucleon axial and pseudoscalar form factors from the covariant Faddeev equation. Eur. Phys. J. A **48**, 9 (2012)
49. P. Maris, C.D. Roberts, π and K meson Bethe-Salpeter amplitudes. Phys. Rev. C **56**, 3369–3383 (1997)
50. A. Bashir, A. Raya, S. Sánchez-Madrigal, C.D. Roberts, Gauge invariance of a critical number of flavours in QED3. Few Body Syst. **46**, 229–237 (2009)
51. S.-X. Qin, L. Chang, Y.-X. Liu, C.D. Roberts, D.J. Wilson, Interaction model for the gap equation. Phys. Rev. C **84**, 042202(R) (2011)
52. S.-X. Qin, C.D. Roberts, Impressions of the Continuum Bound State Problem in QCD. Chin. Phys. Lett. **37**(12), 121201 (2020)
53. P. Maris, P.C. Tandy, QCD modeling of hadron physics. Nucl. Phys. Proc. Suppl. **161**, 136–152 (2006)
54. A. Krassnigg, Excited mesons in a Bethe-Salpeter approach. PoS CONFINEMENT **8**, 075 (2008)
55. S. Navas et al., Review of particle physics. Phys. Rev. D **110**(3), 030001 (2024)
56. G. Eichmann, Nucleon electromagnetic form factors from the covariant Faddeev equation. Phys. Rev. D **84**, 014014 (2011)
57. M. Ding, K. Raya, D. Binosi, L. Chang, C.D. Roberts, S.M. Schmidt, Symmetry, symmetry breaking, and pion parton distributions. Phys. Rev. D **101**(5), 054014 (2020)
58. L. Schlessinger, C. Schwartz, Analyticity as a Useful Computation Tool. Phys. Rev. Lett. **16**, 1173–1174 (1966)
59. L. Schlessinger, Use of Analyticity in the Calculation of Nonrelativistic Scattering Amplitudes. Phys. Rev. **167**, 1411–1423 (1968)
60. R.A. Tripolt, I. Haritan, J. Wambach, N. Moiseyev, Threshold energies and poles for hadron physical problems by a model-independent universal algorithm. Phys. Lett. B **774**, 411–416 (2017)
61. Z.-F. Cui, D. Binosi, C.D. Roberts, S.M. Schmidt, Fresh extraction of the proton charge radius from electron scattering. Phys. Rev. Lett. **127**(9), 092001 (2021)
62. I.Y. Kobzarev, L.B. Okun, Gravitational Interaction of Fermions. Zh. Eksp. Teor. Fiz. **43**, 1904–1909 (1962)
63. O. V. Teryaev, Spin structure of nucleon and equivalence principle – arXiv:hep-ph/9904376
64. S.J. Brodsky, D.S. Hwang, B.-Q. Ma, I. Schmidt, Light cone representation of the spin and orbital angular momentum of relativistic composite systems. Nucl. Phys. B **593**, 311–335 (2001)
65. P.-L. Yin, Y.-Z. Xu, Z.-F. Cui, C.D. Roberts, J. Rodríguez-Quintero, All-Orders Evolution of Parton Distributions: Principle, Practice, and Predictions. Chin. Phys. Lett. Express **40**(9), 091201 (2023)
66. G. Grunberg, Renormalization Group Improved Perturbative QCD, Phys. Lett. B 95 (1980) 70, [Erratum: Phys. Lett. B 110, 501 (1982)]
67. G. Grunberg, Renormalization Scheme Independent QCD and QED: The Method of Effective Charges. Phys. Rev. D **29**, 2315 (1984)
68. Y. L. Dokshitzer, Calculation of the Structure Functions for Deep Inelastic Scattering and $e^+ e^-$ Annihilation by Perturbation Theory in Quantum Chromodynamics. (In Russian), Sov. Phys. JETP 46 (1977) 641–653
69. V.N. Gribov, L.N. Lipatov, Deep inelastic electron scattering in perturbation theory. Phys. Lett. B **37**, 78–80 (1971)
70. L.N. Lipatov, The parton model and perturbation theory. Sov. J. Nucl. Phys. **20**, 94–102 (1975)
71. G. Altarelli, G. Parisi, Asymptotic Freedom in Parton Language. Nucl. Phys. B **126**, 298–318 (1977)
72. Z.F. Cui, M. Ding, J.M. Morgado, K. Raya, D. Binosi, L. Chang, J. Papavassiliou, C.D. Roberts, J. Rodríguez-Quintero, S.M. Schmidt, Concerning pion parton distributions. Eur. Phys. J. A **58**(1), 10 (2022)
73. F.X. Girod et al., Measurement of Deeply virtual Compton scattering beam-spin asymmetries. Phys. Rev. Lett. **100**, 162002 (2008)
74. H.S. Jo et al., Cross sections for the exclusive photon electroproduction on the proton and Generalized Parton Distributions. Phys. Rev. Lett. **115**(21), 212003 (2015)
75. K. Raya, Z.-F. Cui, L. Chang, J.-M. Morgado, C.D. Roberts, J. Rodríguez-Quintero, Revealing pion and kaon structure via generalised parton distributions. Chin. Phys. C **46**(26), 013105 (2022)
76. M. Diehl, Generalized parton distributions. Phys. Rept. **388**, 41–277 (2003)
77. T.-J. Hou et al., New CTEQ global analysis of quantum chromodynamics with high-precision data from the LHC. Phys. Rev. D **103**(1), 014013 (2021)
78. P. Cheng, Y. Yu, H.-Y. Xing, C. Chen, Z.-F. Cui, C.D. Roberts, Perspective on polarised parton distribution functions and proton spin. Phys. Lett. B **844**, 138074 (2023)
79. C. Alexandrou, S. Bacchio, M. Constantinou, J. Finkenrath, K. Hadjiyiannakou, K. Jansen, G. Koutsou, H. Panagopoulos, G. Spanoudes, Complete flavor decomposition of the spin and momen-

tum fraction of the proton using lattice QCD simulations at physical pion mass. Phys. Rev. D **101**(9), 094513 (2020)
80. R.L. Jaffe, Ambiguities in the definition of local spatial densities in light hadrons. Phys. Rev. D **103**(1), 016017 (2021)
81. A. Freese, G.A. Miller, Forces within hadrons on the light front. Phys. Rev. D **103**, 094023 (2021)
82. A. Freese, G.A. Miller, Unified formalism for electromagnetic and gravitational probes: Densities. Phys. Rev. D **105**(1), 014003 (2022)
83. E. Epelbaum, J. Gegelia, N. Lange, U.G. Meißner, M.V. Polyakov, Definition of Local Spatial Densities in Hadrons. Phys. Rev. Lett. **129**(1), 012001 (2022)
84. A. Freese, G.A. Miller, Convolution formalism for defining densities of hadrons. Phys. Rev. D **108**(3), 034008 (2023)
85. F. Özel, P. Freire, Masses, Radii, and the Equation of State of Neutron Stars. Ann. Rev. Astron. Astrophys. **54**, 401–440 (2016)
86. Y.-Z. Xu, K. Raya, Z.-F. Cui, C.D. Roberts, J. Rodríguez-Quintero, Empirical Determination of the Pion Mass Distribution. Chin. Phys. Lett. Express **40**(4), 041201 (2023)
87. M.-L. Du, V. Baru, F.-K. Guo, C. Hanhart, U.-G. Meißner, A. Nefediev, I. Strakovsky, Deciphering the mechanism of near-threshold J/ψ photoproduction. Eur. Phys. J. C **80**(11), 1053 (2020)
88. Y.-Z. Xu, S. Chen, Z.-Q. Yao, D. Binosi, Z.-F. Cui, C.D. Roberts, Vector-meson production and vector meson dominance. Eur. Phys. J. C **81**, 895 (2021)
89. P. Sun, X.-B. Tong, F. Yuan, Near threshold heavy quarkonium photoproduction at large momentum transfer. Phys. Rev. D **105**(5), 054032 (2022)
90. D. Winney et al., Dynamics in near-threshold J/ψ photoproduction. Phys. Rev. D **108**(5), 054018 (2023)
91. L. Tang, Y.-X. Yang, Z.-F. Cui, C.D. Roberts, J/ψ photoproduction: Threshold to very high energy. Phys. Lett. B **856**, 138904 (2024)
92. S. Sakinah, T. S. H. Lee, H.-M. Choi, Dynamical Model of J/Ψ photo-production on the nucleon. Phys. Rev. C **109**(6), 065204 (2024). https://doi.org/10.1103/PhysRevC.109.065204
93. L. Chang, Y.-X. Liu, C.D. Roberts, Y.-M. Shi, W.-M. Sun, H.-S. Zong, Chiral susceptibility and the scalar Ward identity. Phys. Rev. C **79**, 035209 (2009)
94. A. Krassnigg, Survey of J=0,1 mesons in a Bethe-Salpeter approach. Phys. Rev. D **80**, 114010 (2009)
95. P. Maris, P.C. Tandy, The π, K^+, and K^0 electromagnetic form factors. Phys. Rev. C **62**, 055204 (2000)
96. Z.-F. Cui, D. Binosi, C.D. Roberts, S.M. Schmidt, Hadron and light nucleus radii from electron scattering. Chin. Phys. C **46**(12), 122001 (2022)
97. D. Binosi, A. Pilloni, R.-A. Tripolt, Study for a model-independent pole determination of overlapping resonances. Phys. Lett. B **839**, 137809 (2023)
98. Z.-F. Cui, D. Binosi, C.D. Roberts, S.M. Schmidt, D.N. Triantafyllopoulos, Fresh look at experimental evidence for odderon exchange. Phys. Lett. B **839**, 137826 (2023)
99. D. Binosi, C. D. Roberts, Z.-Q. Yao, Hadron Structure: Perspective and Insights. arXiv:2503.05984 [hep-ph], in: 16th Conference on Quark Confinement and the Hadron Spectrum, 2025